The biochemical basis for the cooperative action of microRNAs

Daniel Briskin[a,b,c], Peter Y. Wang[a,b,c], and David P. Bartel[a,b,c,1]

[a]Whitehead Institute for Biomedical Research, Cambridge, MA 02142; [b]HHMI, Whitehead Institute for Biomedical Research, Cambridge, MA 02142; and [c]Department of Biology, Massachusetts Institute of Technology, Cambridge, MA 02139

Edited by Leemor Joshua-Tor, HHMI and Cold Spring Harbor Laboratory, Cold Spring Harbor, NY, and approved June 12, 2020 (received for review November 21, 2019)

In cells, closely spaced microRNA (miRNA) target sites within a messenger RNA (mRNA) can act cooperatively, leading to more repression of the target mRNA than expected by independent action at each site. Using purified miRNA-Argonaute (AGO2) complexes, synthetic target RNAs, and a purified domain of TNRC6B (GW182 in flies) that is able to simultaneously bind multiple AGO proteins, we examined both the occupancies and binding affinities of miRNA-AGO2 complexes and target RNAs with either one site or two cooperatively spaced sites. On their own, miRNA-AGO2 complexes displayed little if any cooperative binding to dual sites. In contrast, in the presence of the AGO-binding region of TNRC6B, we observed strong cooperative binding to dual sites, with almost no singly bound target RNAs and substantially increased binding affinities and Hill coefficients. Cooperative binding was retained when the two sites were for two different miRNAs or when the two sites were bound to miRNAs loaded into two different AGO paralogs, AGO1 and AGO2. The improved binding affinity was attributable primarily to a reduced rate of dissociation between miRNA-AGO complexes and their dual-site targets. Thus, the multivalent binding of TNRC6 enables cooperative binding of miRNA-AGO complexes to target RNAs, thereby explaining the basis of cooperative action.

TNRC6 | GW proteins | microRNA | Argonaute | RISC

MicroRNAs (miRNAs) are ~22-nt RNAs that associate with an Argonaute (AGO) protein to form a complex that directs the posttranscriptional down-regulation of messenger RNA (mRNAs) (1). Within this complex, the miRNA pairs to a site within an mRNA, typically within its 3′ untranslated region (UTR), thereby specifying the mRNA to be repressed, whereas AGO interacts with TNRC6, a scaffold protein that recruits the PAN2/PAN3 and the CCR4/NOT deadenylation complexes to the targeted mRNA.

The consequences of the ensuing deadenylation can differ, depending on the regulatory regime operating in the cells (2). In early embryos, where mRNAs with shorter tails are stable but translated less efficiently, translational repression is observed. In later embryos or postembryonic cells, where mRNAs with shorter tails are decapped more rapidly but translated no less efficiently, mRNA destabilization is observed. Some translational repression, attributable to the action of DDX6 and 4E-T, which can be recruited by the CCR4/NOT complex (3), is sometimes also observed in postembryonic cells, but more rapid mRNA deadenylation followed by more rapid degradation of short-tailed mRNA isoforms explains most of the repression observed for endogenous mRNAs of postembryonic cells (4, 5).

Key to the interaction between AGO and TNRC6 are three tryptophan-binding pockets on the surface of AGO (6). Indeed, the TNRC6 homolog of flies is named GW182 because of its abundant glycine (G) and tryptophan (W) residues. The G and W residues fall primarily in a large, apparently unstructured N-terminal domain of TNRC6, which has three AGO-binding "hotspots" (3, 7). Each of these hotspots has multiple W residues that are flanked by amino acids with small or flexible side chains, which help explain the affinity to AGO (7, 8).

More than 60% of human mRNAs are conserved targets of miRNAs, and on average, each conserved target has four to five preferentially conserved miRNA sites (9). Each of these sites typically has perfect pairing to the miRNA seed (miRNA positions 2 to 7), often supplemented by an additional pair to miRNA position 8 or an A across from miRNA position 1, or both (1).

Analyses of the global effects of miRNAs on mRNA levels indicate that if an mRNA has multiple sites to the same miRNA, then the observed repression ordinarily matches what would be expected if each site acted independently (10). For example, if one site on its own reduces an mRNA level by 30% and the second site reduces it by 20%, the effect of both of them together would be expected to be 44% [1 – (0.7 × 0.8)]. However, when two miRNA sites are close to each other, the observed repression typically exceeds that expected from the independent action of the two sites (10, 11). One study reports that the strongest cooperative action is observed when sites are <40 nt apart (counting the number of nucleotides between the 3′ end of the upstream site and the 5′ end of the downstream site) but >7 nt apart, presumably because at very close distances, binding of one complex occludes binding of the second complex (10). Another study reports that the strongest cooperative action is observed when sites are 13 to 35 nt apart (11). Here we set out to explain the biochemical basis of this cooperative action.

Significance

MicroRNAs (miRNAs) are short RNAs that guide the repression of most human messenger RNAs (mRNAs) and play many important roles in physiology and development. To function, each miRNA associates with an Argonaute (AGO) protein to form a complex in which the miRNA pairs to sites in mRNAs, thereby targeting these mRNAs for repression, and AGO associates with TNRC6, a protein that recruits the mRNA-repression machinery. For previously unknown reasons, repression is often more effective when miRNAs pair to sites close to one another. We find that in the presence of the TNRC6 AGO-binding domain, which can simultaneously bind multiple AGO proteins, miRNA-AGO complexes bind a two-site target RNA with high cooperatively, providing a biochemical explanation for cooperative action in cells.

Author contributions: D.B., P.Y.W., and D.P.B. designed research; D.B. and P.Y.W. performed research; D.B. and P.Y.W. analyzed data; and D.B., P.Y.W., and D.P.B. wrote the paper.

The authors declare no competing interest.

This article is a PNAS Direct Submission.

[1]To whom correspondence may be addressed. Email: dbartel@wi.mit.edu.

This article contains supporting information online at https://www.pnas.org/lookup/suppl/doi:10.1073/pnas.1920404117/-/DCSupplemental.

First published July 13, 2020.

Results and Discussion

In Vitro Analysis of miRNA Site Occupancy. Recent experiments show that repression efficacy correlates strongly with the binding affinity between the miRNA-AGO complex and its target sites (12). Accordingly, we reasoned that the cooperative action of closely spaced sites might be due to cooperative binding of miRNA-AGO complexes to two closely spaced sites. To test this idea, we examined whether the miRNA-AGO complex binds cooperatively to an RNA target with two closely spaced sites.

Bulk binding affinities between miRNA-AGO complexes and their targets are typically measured using filter binding, in which a nitrocellulose membrane retains AGO and any associated RNA, thereby separating bound from unbound target RNA (13). However, because this method cannot distinguish target RNA bound by one complex from that bound by two complexes, it cannot provide the occupancy information needed to measure binding cooperativity. Reasoning that a native electrophoretic mobility-shift assay (EMSA) would be able to provide the desired occupancy information, we explored the utility of this assay for examining binding affinity between the miR-1–AGO2 complex and its targets.

We first measured the binding affinity between the complex and an RNA with a single site. Human AGO2 loaded with human miR-1 was purified (12, 14), and its binding to a 27-nt RNA that had a site matching miR-1 nucleotides 2 to 8 (Fig. 1*A*) was examined. A range of miR-1–AGO2 concentrations were incubated with trace target RNA, which was 5′-radiolabeled, and after reaching binding equilibrium, the fraction of bound target was measured by both a filter-binding assay and a native EMSA. The filter-binding assay was performed with stacked nitrocellulose and nylon membranes, in which the nitrocellulose membrane captured AGO and any associated RNA, and the nylon captured unbound RNA (Fig. 1*B*). At each AGO2 concentration, the fraction of bound target observed by EMSA resembled that observed by filter binding (Fig. 1 *B* and *C*). For both assays, simple binding curves fit well to the results, and the K_D values inferred from these curves (91 and 110 pM, respectively) were similar to each other (Fig. 1*D*) and fell within the range of values determined for complexes involving other mammalian miRNAs and measured using either filter-binding or single-molecule methods (13, 15).

Having established an EMSA for miR-1–AGO2 binding to target RNA, we used this assay to examine binding to a target with two 7-nt sites separated by 21 nt, choosing an oligo(U) spacer to avoid secondary structures within the target RNA (Fig. 1*A*). As anticipated, EMSA distinguished between free RNA, RNA bound by one miR-1–AGO2 complex, and RNA bound by two miR-1–AGO2 complexes, and when considering the fraction of target bound to at least one complex, results of the EMSA agreed well with those of the filter-binding assay (Fig. 1 *E*–*G*).

The distinctly identifiable binding states observed with the EMSA allowed fitting of the Hill equation, producing a Hill coefficient, h, used to describe the cooperativity of binding in systems with multiple simultaneous binding events. An h of 1.0 indicates no cooperativity, whereas an h <1.0 or >1.0 indicates negative or positive cooperativity, respectively. Because the target had two miRNA target sites, an h of 2 would indicate maximal positive cooperativity. Fitting the Hill equation to the EMSA results for a two-site target yielded an h of 1.2, with a 95% confidence interval (CI) of 0.96 to 1.5 (Fig. 1*H*). Thus, although the possibility of some cooperative binding could not be excluded, these results did not provide compelling evidence for the cooperative binding of miR-1–AGO2 to a two-site target in the absence of additional factors.

Enhanced Cooperativity of AGO2 Binding in the Presence of TNRC6. TNRC6 has an extended AGO-binding domain with the potential to bind more than one AGO (16). Indeed, within the AGO-binding domain of TNRC6B, one of the three TNRC6 paralogs in humans, three nonoverlapping AGO-binding hotspots have been mapped (7), and one molecule of TNRC6A can simultaneously bind three AGO proteins (8). This ability to bind more than one AGO protein has led to speculation that TNRC6 might link multiple miRNA-AGO complexes simultaneously bound to different sites of a target, thereby imparting cooperative binding to such targets with multiple suitably spaced sites (7, 8, 16, 17).

With an assay for examining the cooperativity of miRNA-AGO binding to targets, we were positioned to test the idea that the AGO-binding domain of TNRC6 might impart cooperative binding. For these studies, we overexpressed and purified the AGO-binding domain of TNRC6B. The recombinant construct, named 6B-ABD, included a region of TNRC6B containing residues 162 to 996, fused at its N terminus with maltose-binding protein (MBP) and at its C terminus with His_6, which were appended to enhance protein solubility and facilitate purification, respectively (Fig. 2*A*).

To examine how binding of 6B-ABD affected migration of miRNA-AGO2-target complexes, we designed a system that enabled control of the number of target sites bound to miRNA-AGO2. This system used a target with two different sites: one site that bound miR-1 and another that bound miR-124, again separated by a 21-nt oligo(U) spacer. To this two-site target, purified miR-124–AGO2 or miR-1–AGO2 could be added to generate a singly bound target, or both miRNA-AGO2 complexes could be added to generate a doubly bound target (Fig. 2*B*). 6B-ABD was then added to these singly or doubly bound targets, and migration in the EMSA was assessed (Fig. 2*B*). Adding 1 nM 6B-ABD to a target bound by either a single miR-1–AGO2 or a single miR-124–AGO2 reduced the mobility of the target complex only slightly, whereas adding 1 nM 6B-ABD to a target bound by both miR-1–AGO2 and miR-124–AGO2 substantially reduced the mobility of the target complex, a small portion of which failed to migrate into the gel. These results demonstrated the ability to detect association of 6B-ABD to target bound by two miRNA-AGO2 complexes.

Having established how adding 6B-ABD influences the migration of different miRNA-AGO2-target complexes, we next investigated how 6B-ABD influences the binding of miR-1–AGO2 to its two-site target RNA. Compared with binding reactions without 6B-ABD (Fig. 1*B*), adding 1 nM 6B-ABD nearly eliminated the singly bound species (Fig. 2*C*), with the doubly bound target dominating over the singly bound target at much lower miR-1–AGO2 concentrations (as low as 6 pM, compared to >60 pM). This altered behavior observed after addition of the TNRC6B AGO-binding domain was precisely that expected when shifting from noncooperative to highly cooperative binding. Indeed, when fitting the Hill equation, the occupancy observed after adding 6B-ABD yielded an h of 2.1 (95% CI, 1.5 to 3.2) (Fig. 2*D*). We conclude that TNRC6 substantially increases the cooperativity of miR-1–AGO2 binding to a two-site target RNA.

To examine whether the observed cooperativity depends on the identity of the miRNA, we repeated the experiments with miR-124–AGO2 and a cognate target with two sites to miR-124 separated by a 21-nt oligo(U) spacer. The results resembled those observed for miR-1; the singly bound species observed without 6B-ABD was nearly undetectable in the presence of 6B-ABD, and the doubly bound target dominated over the singly bound target at much lower miR-124–AGO2 concentrations (Fig. 2 *E* and *F*). In the absence of 6B-ABD, the Hill coefficient was 1.3 (95% CI, 1.0 to 1.7), which increased to 1.8 (95% CI, 1.5 to 2.2) with the addition of 6B-ABD (Fig. 2*G*).

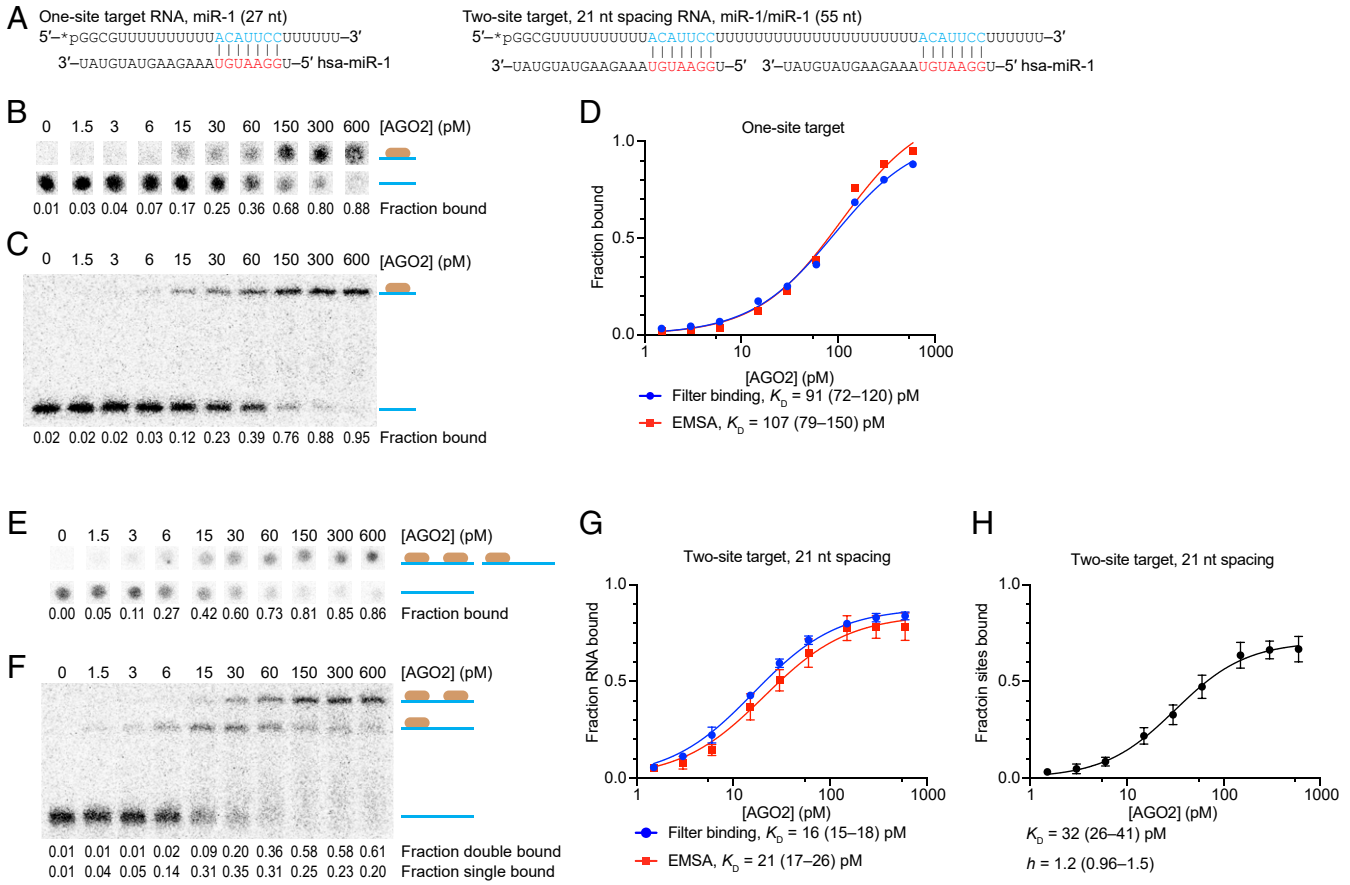

Fig. 1. Binding of miR-1–AGO2 to targets with either one or two sites. (*A*) Diagram of synthetic miR-1 targets with either one site or two sites. The 7-nt sites (blue) pair to miRNA positions 2 to 8 (red). (*B*) Binding of miR-1–AGO2 to its one-site target, as detected by filter binding. The top row shows the amount of labeled target retained with miR-1–AGO2 on the nitrocellulose filter, with the cartoon on the right depicting the miRNA-AGO-target ternary complex (brown AGO2 bound to blue target). The bottom row shows the amount of labeled target that passed through the nitrocellulose filter and bound to the nylon filter, with the cartoon depicting the free target (blue line). Shown are phosphorimager scans of the filters, which were used to calculate the fraction of target bound (indicated below the scans) for each concentration of miR-1–AGO2. (*C*) Binding of miR-1–AGO2 to its one-site target, as detected by EMSA. Otherwise, this panel is as in *B*. (*D*) Binding curves fit to the results of *B* and *C* (blue and red, respectively). Shown for each method are inferred K_D values with 95% CIs in parentheses. (*E*) Binding of miR-1–AGO2 to its two-site target as detected by filter binding. The cartoons on the right depict two AGO2 complexes bound to the target (*Top Left*), one AGO2 complex bound to the target (*Top Right*, shown bound to one site but also could be bound to the other site), and free target (*Bottom*). Otherwise, this panel is as in *B*. (*F*) Binding of miR-1–AGO2 to its two-site target, as detected by EMSA. Otherwise, this panel is as in *E*. (*G*) Binding curves fit to three replicates of both *E* and *F* (blue and red, respectively). Otherwise, this panel is as in *D*. (*H*) The Hill curve fit to three replicates of *F*, showing the K_D and *h* values, with 95% CIs in parentheses.

Cooperativity Involving Different miRNAs and Different AGO Paralogs. Because most cooperatively spaced sites in endogenous 3′ UTRs correspond to different miRNAs, we also tested whether the TNRC6B AGO-binding domain could enhance cooperative binding to the target used earlier to examine the migration of 6B-ABD–bound complexes (Fig. 2*B*), which had sites to the two different miRNAs. miR-124–AGO2 was set at 30 pM, a concentration that led to partial occupancy of the miR-124 site, and miR-1–AGO2 was titrated in, in either the absence or the presence of 6B-ABD (Fig. 3 *A* and *B*). Clear hallmarks of increased cooperativity were observed in the presence of 6B-ABD; for example, at 30 pM miR-124–AGO2, 15 pM miR-1–AGO2, and in the absence of 6B-ABD, 68% of target RNA was free, 19% was bound by one miRNA–AGO2 complex, and 13% was bound by two complexes, whereas in the presence of 6B-ABD, free target decreased to 18%, singly bound target decreased to 17%, and doubly bound target increased to 65% (Fig. 3 *A* and *B*). Thus, TNRC6 can mediate cooperative binding involving two AGO proteins, each loaded with a unique miRNA.

This RNA target with sites to two different miRNAs also allowed us to assess whether TNRC6 would impart cooperative binding when the miRNAs were loaded within different AGO paralogs. Four AGO paralogs, AGO1–4, are expressed in humans, each of which has been suggested to bind to TNRC6 (7, 8, 16, 17). To investigate whether TNRC6 can mediate cooperative binding involving two different AGO paralogs, we repeated the experiment with miR-124 loaded into AGO1 and miR-1 loaded into AGO2. miR-124–AGO1 was set at 30 pM for partial occupancy of the miR-124 site, and miR-1–AGO2 was titrated in, with or without 6B-ABD (Fig. 3*C*). Again, the binding patterns exhibited clear hallmarks of increased cooperativity in the presence of 6B-ABD. At 30 pM miR-124–AGO1, 10 pM miR-1–AGO2, and no 6B-ABD, 49% of target RNA was free, 35% was singly bound by miRNA-AGO1/2, and 16% was doubly bound. With 1 nM 6B-ABD, only 13% was free, 9% was singly bound, and 78% was doubly bound (Fig. 3*C*).

Taken together, these results dramatically expanded the implied scope of TNRC6-mediated cooperative binding beyond sites for the same miRNA-AGO complex to include a far greater number of appropriately spaced sites for different coexpressed miRNAs loaded within the same or different AGO paralogs. Moreover, because TNRC6 can simultaneously bind three AGO

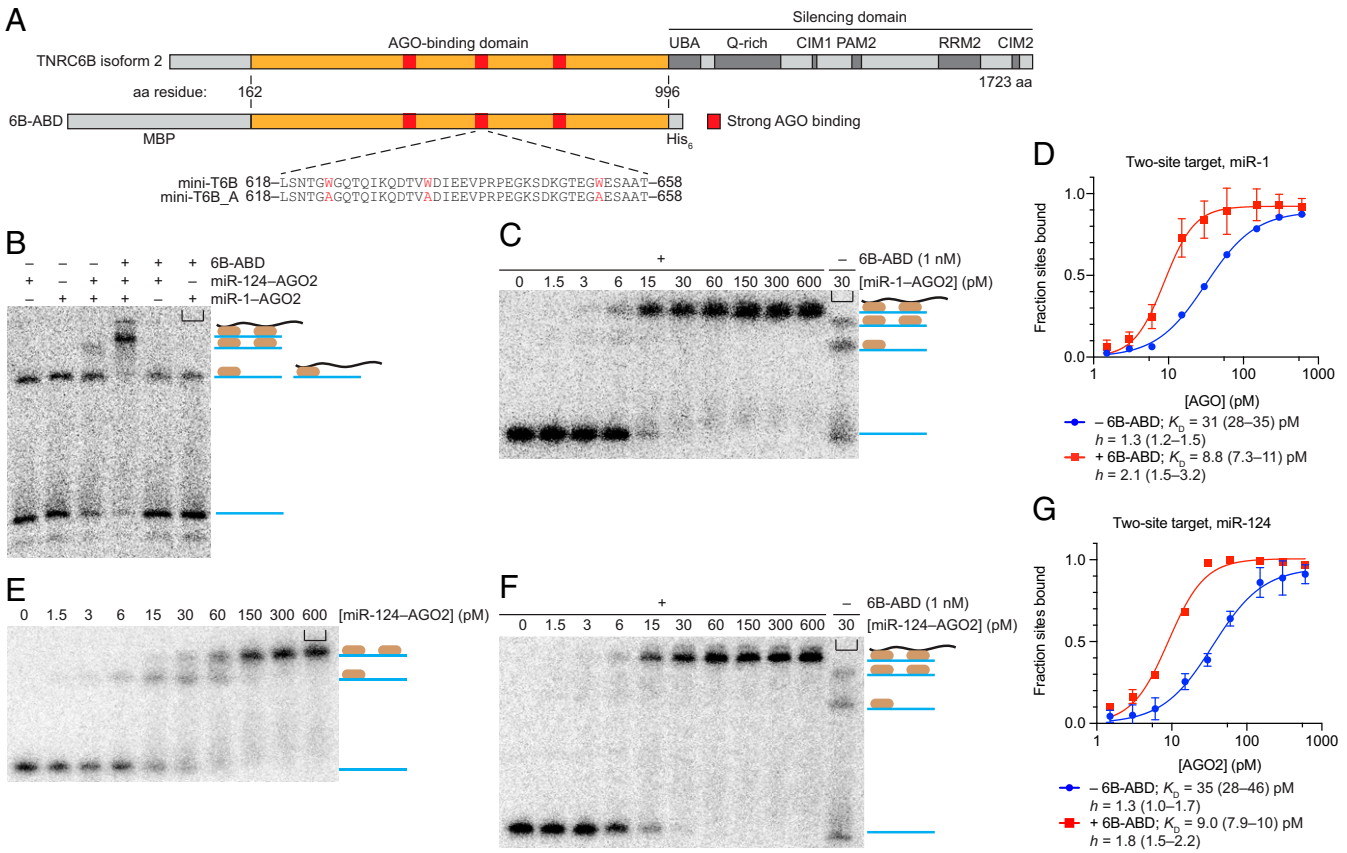

Fig. 2. The effects of 6B-ABD on miRNA-AGO2 binding to two-site targets. (*A*) Domain structure of TNRC6B and its derivatives. At the top is TNRC6B isoform 2, with its AGO-binding domain in orange and the mapped high-affinity binding regions in red. Below TNRC6B is 6B-ABD, which contains the TNRC6B AGO-binding domain flanked by the MBP and a His_6 tag. Below 6B-ABD are the mini-T6B and mini-T6B_A synthetic peptides. (*B*) Assessment of target migration in the EMSA following combinatorial addition of miRNA-AGO and 6B-ABD. On the right, cartoons depict (*Top* to *Bottom*): target (blue) bound by two miRNA-AGO2 complexes (brown) that are bound by 6B-ABD (black), target bound by two miRNA-AGO2 complexes, target bound by one miRNA-AGO2 complex (either miR-1–AGO2 or miR-124–AGO2, but only one of these two possibilities is shown for simplicity), and target bound by one miRNA-AGO2 complex that is bound by 6B-ABD (which essentially comigrates with target bound by one miRNA-AGO2 complex that is not bound by 6B-ABD), and free target. The three-sided box in *Upper Right* corner of the gel shows the location of the well. (*C*) The effect of 6B-ABD on the binding of miR-1–AGO2 to its two-site target. 1 nM 6B-ABD was included in each binding reaction, except the reaction run on the far-right lane. Cartoons on the right are as in *B*. Otherwise, this panel is as in Fig. 1*F*. (*D*) The effect of 6B-ABD on the binding of miR-1–AGO2 to its two-site target, as evaluated by the Hill equation. The Hill equation is fit to two replicates of *C* (red) and to EMSA results for the analogous binding reactions performed in the absence of 6B-ABD (blue). K_D and h values are indicated for each fit, with 95% CIs in parentheses. (*E*) Binding of miR-124–AGO2 to its two-site target. Otherwise, this panel is as in Fig. 1*F*. (*F*) The effect of 6B-ABD on the binding of miR-124–AGO2 to its two-site target. Otherwise, this panel was as in *C*. (*G*) Hill equation fit to two replicates of *E* and *F* (blue and red, respectively). Otherwise, this panel is as in *D*.

molecules (10, 11), we anticipate that cooperativity occurring at three appropriately spaced sites would be even greater than that occurring at two appropriately spaced sites.

Site Spacing. Previous studies examining the efficacy of repression in the cell indicate that either 8 to 39 nt or 13 to 35 nt between the 3′ end of the first site and the 5′ end of the second site provides optimal spacing for miRNA cooperative action (10, 11), raising the question of whether such a range also applies to binding cooperativity in vitro. To test intersite spacing above the previously defined boundaries, we created a target with a 60-nt oligo(U) spacer. Using this target in the absence of 6B-ABD, three binding states were observed: free target, target bound by a single miR-1–AGO2 complex, and target bound by two miR-1–AGO2 complexes (Fig. 4*A*), whereas in the presence of 6B-ABD, target bound by a single miR-1–AGO2 complex was difficult to detect at any point in the concentration course—a hallmark of cooperative binding (Fig. 4*B*). Fitting the binding curves indicated that in the absence of 6B-ABD, miR-1–AGO2 bound target RNA with K_D = 24 pM and h = 1.4 (95% CI, 0.94 to 2.0), whereas in the presence of 6B-ABD, miR-1–AGO bound target RNA with K_D = 9.1 pM and h = 1.8 (95% CI, 1.3 to 2.6) (Fig. 4*C*), also supporting the conclusion that 6B-ABD increased the affinity and cooperativity of binding.

These results show that cooperative binding can be achieved at a linker length of 60 nt, which exceeds the 56-nt linker length for which cooperativity is not observed in cells using a reporter assay (10). Factors that might explain this difference include the different linker and flanking sequences and the milieu of RNA-binding proteins present in cells but absent in our purified system, which might effectively iron out the target mRNA and increase the mean distance between sites.

To test an intersite spacing below the previously defined boundaries, we generated a two-site target with an miR-1 site placed 4 nt from a miR-124 site. In the absence of 6B-ABD, binding of only one miRNA-AGO2 complex to the target was detected, with a K_D of 88 pM, whereas in the presence of 6B-ABD, the same was observed, with a similar K_D of 140 pM (Fig. 4 *D*–*F*). The binding of only one miRNA-AGO2 complex to this target with closely spaced sites was presumably due to a

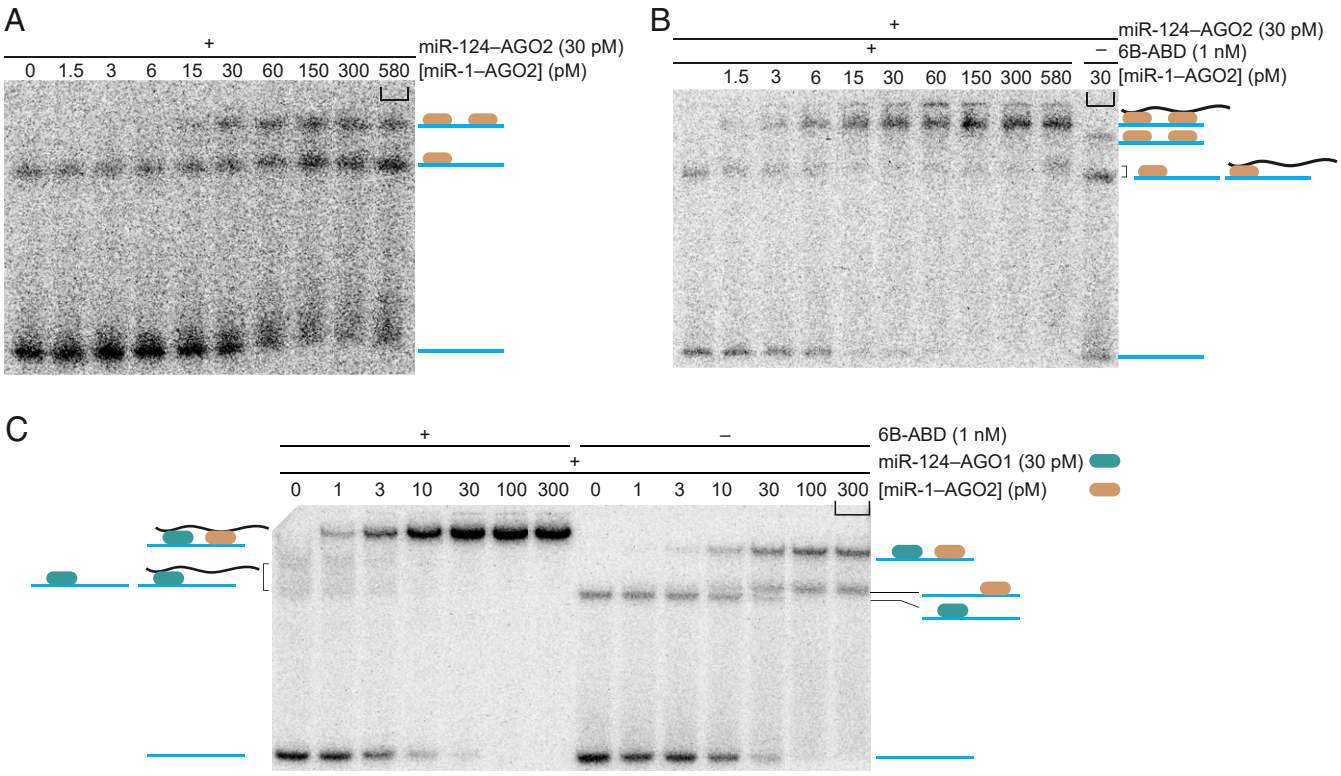

Fig. 3. The effects of 6B-ABD on binding of different miRNAs to the same target and on binding of miRNAs loaded into different AGO paralogs. (*A*) Binding of miR-1–AGO2 and miR-124–AGO2 to a target with one site to each miRNA. miR-1–AGO2 was titrated into reactions containing 30 pM miR-124–AGO2. Otherwise, this panel is as in Fig. 2*E*. (*B*) The effect of 6B-ABD on the binding of miR-1–AGO2 and miR-124–AGO2 to a target with one site to each miRNA. miR-1–AGO2 was titrated into reactions containing 30 pM miR-124–AGO2. Otherwise, this panel is as in Fig. 2*C*. (*C*) The effect of 6B-ABD on the binding of miR-1–AGO2 and miR-124–AGO1 to a target with one site each to each miRNA-AGO complex. miR-1–AGO2 (brown) was titrated into reactions containing 30 pM miR-124–AGO1 (teal). Otherwise, this panel is as in *B*.

steric clash that precluded binding of a second complex. This apparent inability of two AGO proteins to simultaneously associate with the target explained the lack of cooperative binding. This mechanism for preventing cooperativity presumably would be difficult to attenuate with altered sequences or RNA-binding proteins, which explains why our result in vitro matched that observed for closely spaced sites when using reporter assays in cells (10, 11).

Disrupting Cooperative Binding. 6B-ABD had the three known AGO-binding hotspots of TNRC6B, consistent with the hypothesis that the ability of 6B-ABD to bind multiple AGO proteins simultaneously provided the basis for cooperative binding of AGO to target RNA. To evaluate this hypothesis that cooperativity depended on multiple and specific AGO–TNRC6 interactions, we generated a synthetic peptide designed to bind only one AGO protein and examined whether this peptide could disrupt cooperative binding. Our peptide was a smaller version of the T6B peptide, an 85-aa peptide that corresponds to residues 599 to 683 of TNRC6B and is known to bind strongly to AGO (7, 17) (Fig. 2*A*). Our peptide, called "mini-T6B," included a 41-aa fragment of T6B corresponding to residues 618 to 658 of TNRC6B. Mini-T6B was designed to include only three tryptophan residues, with the reasoning that such a peptide could interact with each of the tryptophan-binding pockets on one AGO molecule but would lack additional tryptophan residues that might interact with another AGO. As a control, a second peptide, called "mini-T6B_A," was designed in which the three tryptophan residues of mini-T6B were changed to alanine (Fig. 2*A*).

The effect of mini-T6B was tested on miR-1–AGO2 binding to a target with two miR-1 sites spaced 21 nt apart (Fig. 1*B*), setting the concentration of miR-1–AGO2 to 30 pM, at which free target RNA, target RNA bound by one miR-1–AGO2 complex, and target RNA bound by two miR-1–AGO2 complexes were clearly observed. When adding a high concentration of mini-T6B or mini-T6B_A to the reaction, neither peptide affected the mobility of the complexes (Fig. 5*A*); however, in the presence of 1 nM 6B-ABD, which normally imparts cooperative binding of miR-1–AGO2, adding mini-T6B disrupted the cooperative behavior, as indicated by the reappearance of singly bound target (Fig. 5 *B* and *C*). Adding mini-T6B–A did not disrupt the cooperative behavior, as would be expected if the behavior were mediated specifically through tryptophan residues binding to AGO2. These results support the conclusion that simultaneous binding of TNRC6 to multiple miRNA-AGO2 complexes enables cooperative binding to targets that have suitably spaced miRNA sites. Moreover, the high concentration of mini-T6B required to displace 6B-ABD from the two-site target bound by two miRNA-AGO complexes indicates that the affinity between 6B-ABD and the doubly bound two-site target is much greater than the affinity between mini-T6B and the doubly bound two-site target. This greater affinity can be explained by higher avidity conferred by the multiple high-affinity AGO-binding regions found within 6B-ABD.

TNRC6 Slows Dissociation between miRNA-AGO2 and Its Dual-Site Target. TNRC6 might impart cooperative binding by increasing the association rate constant (k_{on}) between miRNA-AGO and the target, slowing the dissociation rate constant (k_{off}), or both.

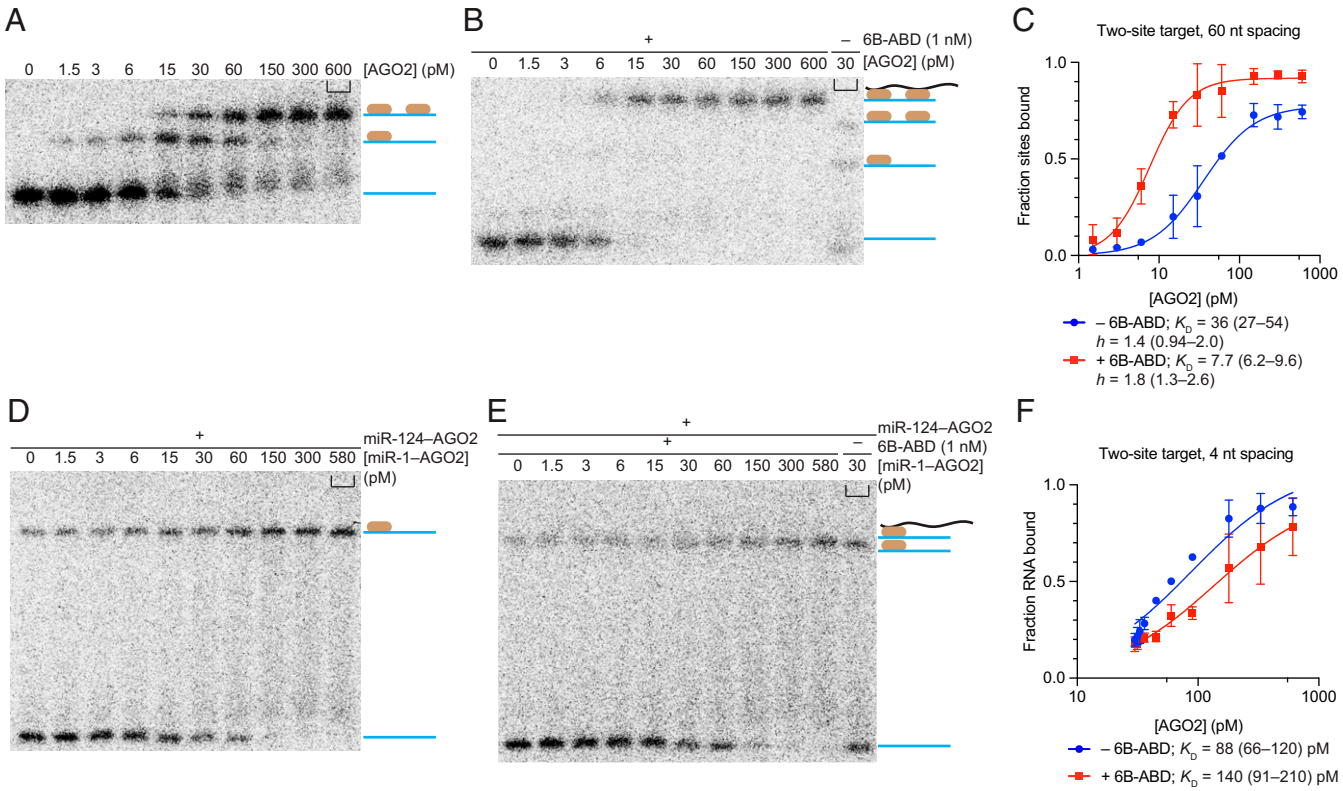

Fig. 4. Assessing cooperative binding at different site-spacing distances. (*A*) Binding of miR-1–AGO2 to a target with two sites spaced 60 nt apart, as detected by EMSA. Otherwise, this panel is as in Fig. 1*E*. (*B*) The effect of 6B-ABD on the binding of miR-1–AGO2 to a target with two sites spaced 60 nt apart. Otherwise, this panel was as in Fig. 2*C*. (*C*) The effect of 6B-ABD on the binding of miR-1–AGO2 to a target with two sites spaced 60 nt apart, as evaluated by the Hill equation. The Hill equation was fit to two replicates of *A* and *B* (blue and red, respectively). Otherwise, this panel is as in Fig. 2*D*. (*D*) Binding of miR-1–AGO2 and miR-124–AGO2 to a target with closely spaced sites to each miRNA. miR-1–AGO2 was titrated into reactions containing 30 pM miR-124–AGO2. Otherwise, this panel is as in Fig. 3*A*. (*E*) The effect of 6B-ABD on the binding of miR-1–AGO2 and miR-124–AGO2 to a target with closely spaced sites to each miRNA. Target bound by one miRNA–AGO2 complex (either miR-1–AGO2 or miR-124–AGO2 but only one of the two possibilities shown for simplicity) migrates slightly faster than target bound by one miRNA–AGO2–6B-ABD complex. Otherwise, this panel is as in Fig. 3*B*. (*F*) Binding curves fit to two replicates of *D* and *E* (blue and red, respectively). Shown for each curve are inferred K_D values with 95% CIs in parentheses.

To distinguish among these possibilities, we assessed the effects of 6B-ABD on these rate constants.

First, to test the effect on k_{on}, we developed an assay in which two slicing substrates competed for binding to the miRNA-AGO complex, such that their relative slicing rates were sensitive to differences in k_{on} but not to differences in k_{off}. One of the two slicing substrates was a 22-nt RNA that was perfectly complementary to miR-1 and thus could be sliced by miR-1–AGO2

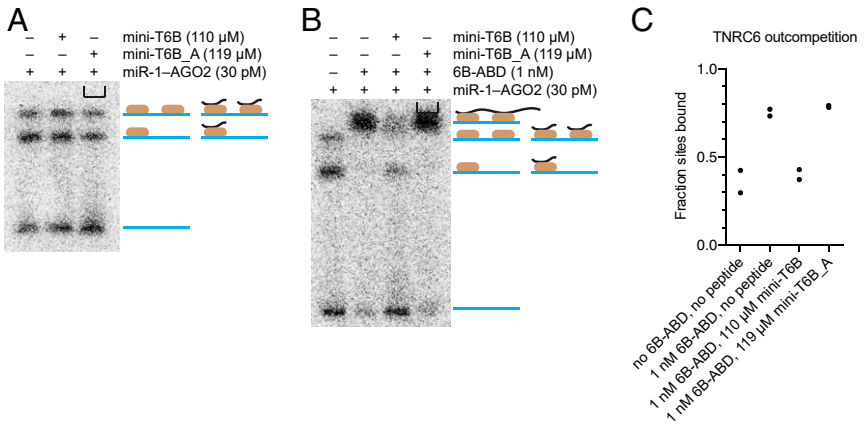

Fig. 5. Disrupting cooperative binding. (*A*) The effect of mini-T6B or mini-T6B_A on the binding of miR-1–AGO2 to its two-site target with 21 nt between sites. In cartoons, the short black line represents mini-T6B1 or mini-T6B_A. Otherwise this panel in as in Fig. 1*F*. (*B*) The effect of mini-T6B or mini-T6B_A on the binding of miR-1–AGO2 to its two-site target in the presence of 1 nM 6B-ABD. In cartoons, short black line represents mini-T6B1 or mini-T6B_A. Otherwise, this panel is as in Fig. 2*C*. (*C*) Quantification of two replicates of *B*.

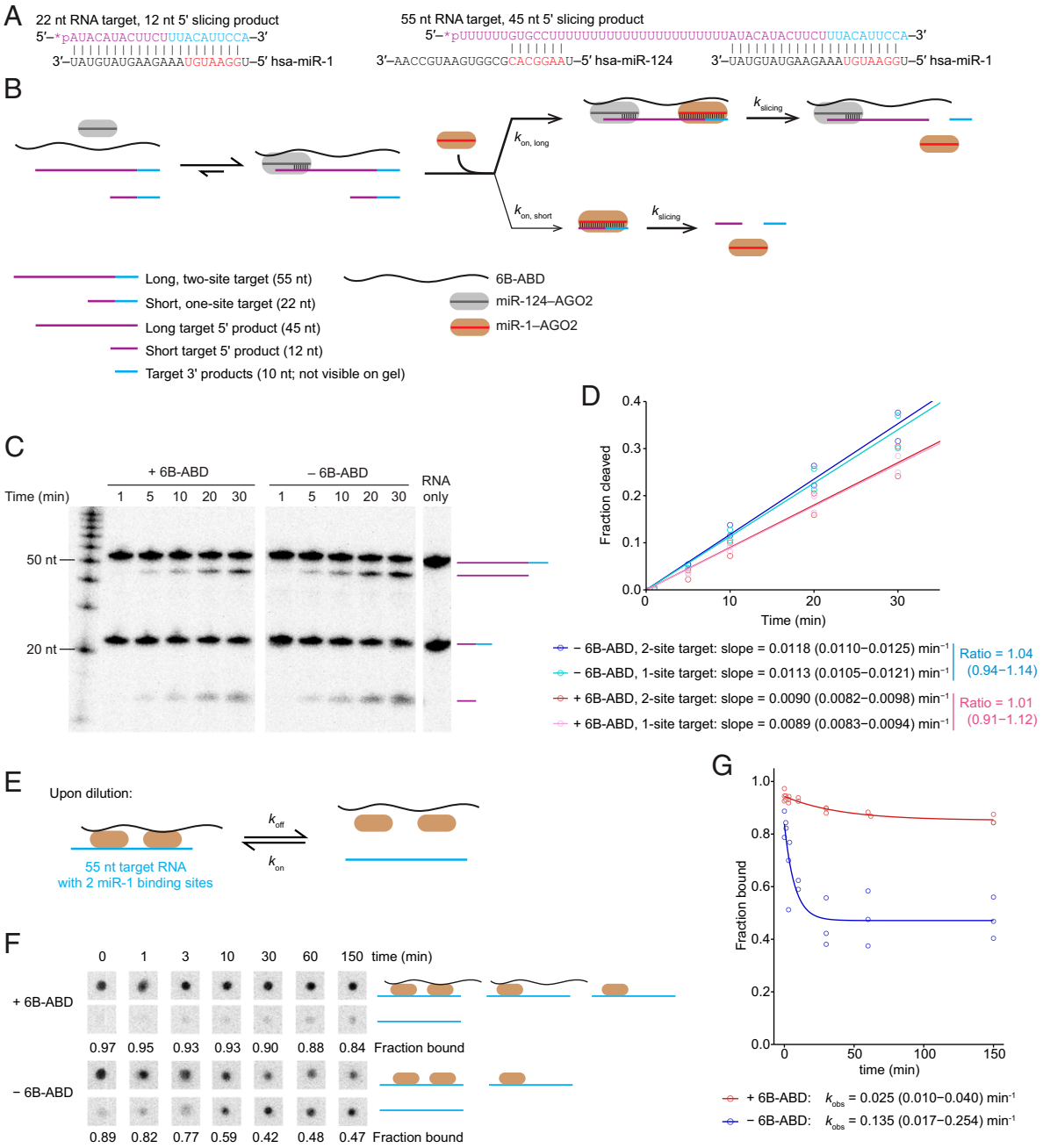

Fig. 6. TNRC6 has little effect on association but slows dissociation of cooperatively bound miRNA-AGO2 complex. (*A*) Diagram of targets used in the competitive-slicing assay. The longer, two-site slicing target has two miRNA sites spaced 20 nt apart. The 5′ site is designed to bind miR-124–AGO2, whereas the 3′ site is designed to bind and be sliced by miR-1–AGO2. Slicing of this target generates a 45-nt 5′ product (purple) and a 10-nt 3′ product (blue). The one-site slicing target has one miR-1 binding and slicing site. Slicing generates a 12-nt 5′ product (purple) and 10-nt 3′ product. (*B*) Schematic of a competitive-slicing assay designed to detect an influence of 6B-ABD on the association of miRNA-AGO2 and target. The two targets are mixed and incubated with 6B-ABD and miR-124–AGO2, using a 6B-ABD concentration that promotes cooperative binding and a miR-124–AGO2 concentration that is in excess and substantially above its K_D for the 7-nt site. After allowing for binding equilibrium, limiting miR-1–AGO2 is added. If 6B-ABD enhances the association rate constant (k_{on}) of miRNA–AGO2, then in the presence of 6B-ABD, miR-1–AGO2 would preferentially associate with the two-site target already bound with miR-124–AGO2 (thicker arrow). Once associated with target, binding is irreversible, because slicing occurs much more rapidly than dissociation. Thus, to the extent that 6B-ABD enhances k_{on}, slicing generates more 45-nt product than 12-nt product. For simplicity, miR-1–AGO2 complexes are shown as dissociated from sliced products. (*C*) Results of a competitive-slicing experiment diagramed in *B*. miR-124–AGO2 was incubated in fivefold excess over 5′-radiolabeled one-site and two-site targets, with or without 6B-ABD. After 2 h, miR-1–AGO2 was added to reach a final concentration of 250 pM miR-124–AGO2, 50 pM each target, 5 pM miR-1–AGO2. At the times indicated, the reaction was stopped, and targets and products were resolved on a denaturing gel. Shown is a phosphorimager scan of the gel. Left lane, decade RNA ladder. Cartoons of labeled RNA species to the right of gel are as in *B*. (*D*) Quantification of the results of the competitive-slicing experiment, indicating that 6B-ABD does not detectably increase the k_{on} for the two-site target. Lines show the linear fit (with slope and 95% CI indicated) to the results in *C*, together with those of a second replicate. (*E*) Schematic of the dilution assay used to investigate differences in k_{off} values. The miR-1–AGO2 complex is incubated with its 55-nt two-site RNA target (Fig. 1*A*) using concentrations in which most target is bound. On dilution, a new equilibrium is established in which more of the bound RNA dissociates into free RNA and protein components. (*F*) Fraction of target RNA bound to miR-1–AGO2 at time points following dilution, as detected by filter binding. The cartoons on the right depict molecular species as in Fig. 2*C*. Otherwise, this panel is as in Fig. 1*B*. (*G*) Exponential curves fitting the approach to the new equilibrium for three replicates of *F*. Shown for each curve are the fitted values for k_{obs}, with 95% CIs in parentheses.

(Fig. 6*A*). The other substrate was a 55-nt RNA that, in addition to having a site perfectly complementary to miR-1, also had a site complementary to nucleotides 2 to 8 of miR-124, separated from the miR-1 site by a 20-nt oligo(U) linker (Fig. 6*A*). The two substrates were combined and preincubated with excess miR-124–AGO2, which could bind but not slice the two-site target, in either the presence or absence of 6B-ABD. Once binding equilibrium was reached, limiting miR-1–AGO2 was added, such that each target RNA was in 10-fold excess over the added miR-1–AGO2. In this regime, the two substrates were competing for binding to miR-1–AGO2, and because slicing of the perfectly complementary site is much more rapid than dissociation of miR-1–AGO2 from this perfectly complementary site (13, 18), binding was essentially irreversible, and the binding competition was based primarily on relative association rates. Thus, if pre-associated 6B-ABD could act to increase the k_{on} of miR-1–AGO2 to the two-site target, then the presence of 6B-ABD would be expected to enhance binding to, and slicing of, the two-site target compared with the one-site target (Fig. 6*B*). However, if 6B-ABD could not act to increase the k_{on} of miR-1–AGO2 to the two-site target, then the presence of 6B-ABD would not be expected to influence the slicing of the two-site target compared with the one-site target. We observed that 6B-ABD did not preferentially enhance slicing of the two-site target; the ratio of the slicing rate of the two-site target to that of the one-site target was 1.01 in the presence of 6B-ABD, compared with 1.04 in the absence of 6B-ABD (Fig. 6 *C* and *D*). Instead, 6B-ABD slightly decreased slicing of both targets (Fig. 6 *C* and *D*).

This undetectable influence on k_{on} implies that the TNRC6 confers greater affinity primarily by slowing the k_{off} between miRNA-AGO and the two-site target. To test this possibility, we measured dissociation kinetics by examining how rapidly binding reactions reached new equilibria following dilution. The 55-nt target with two sites complementary to nucleotides 2 to 8 of miR-1 was incubated with miR-1–AGO2 with or without 6B-ABD, using a target concentration below the K_D and a miR-1–AGO2 concentration above the K_D yet sensitive to dilution even in the presence of 6B-ABD (Fig. 6*E*). Once the initial binding equilibrium was achieved, each reaction mixture was diluted 20-fold while maintaining the 6B-ABD concentration, and filter binding was used to monitor the fraction of RNA bound as the reaction approached its new equilibrium (Fig. 6*E*). This dilution did not include a chase with unlabeled target RNA, out of concern that this extra target RNA might bind to a miRNA-AGO2 of a partially dissociated $(\text{miRNA-AGO2})_2$–6B-ABD complex, which would allow the unlabeled target to gain a toehold to displace the labeled target and thereby cause its more rapid dissociation. Owing to experimental constraints, binding reactions were not diluted to negligible binding of RNA at final equilibrium.

The presence of 6B-ABD slowed the rate at which the binding reaction reequilibrated, with the rate constant (k_{obs}) of reequilibration decreasing from a value of 0.135 min^{-1} (95% CI, 0.017 to 0.254 min^{-1}) in the absence of 6B-ABD to a value of 0.025 min^{-1} (95% CI, 0.010 to 0.040 min^{-1}) in the presence of 6B-ABD (Fig. 6 *F* and *G*). Because a slower dissociation rate would reduce k_{obs}, these results imply slower dissociation in the presence of 6B-ABD. An alternative explanation for a reduced k_{obs} value would be a slower association rate in the presence of 6B-ABD, but when considering that the reaction that included 6B-ABD reached a much higher final level of bound RNA compared with the reaction that omitted 6B-ABD (Fig. 6 *F* and *G*), this explanation would require even more disparate dissociation rate constants. Indeed, simulations probing the relationship between k_{off} and k_{obs} under different regimes of k_{on} and k_{off} implied an even greater difference in the true k_{off} values than suggested by the difference in k_{obs} values (*SI Appendix*, Fig. S1).

Taken together, our results indicate that the primary cause of the cooperative binding observed in the presence of 6B-ABD is slowed k_{off} between miRNA-AGO and its target with suitably spaced sites. Thus, TNRC6 helps maintain the binding of two miRNA-AGO complexes to a two-site target once they are already associated but does little to help recruit the second miRNA-AGO complex to the second site of a target. The notion that multivalent binding of TNRC6 to miRNA-AGO is consequential primarily only after the miRNA-AGO complexes have already associated with target would be even more relevant in the cell, where the high diversity of miRNAs would lower the probability that the second miRNA-AGO complex that might interact with TNRC6 before interacting with the target would also happen to match the second target site.

Model for the Cooperative Binding and Cooperative Action of miRNAs. Our results point to a model in which TNRC6 confers cooperative binding of miRNA-AGO to appropriately spaced sites on target mRNAs (Fig. 7). In this model, individual miRNA-AGO complexes first bind target RNA, typically without the help of TNRC6, and then TNRC6 associates with these target-bound miRNA-AGO proteins. Although TNRC6 does not change the microscopic dissociation rate of an individual miRNA-AGO bound to its site, it does help keep the miRNA-AGO close to the target, such that if one of the two miRNA-AGO complexes dissociates from its site, then TNRC6 in conjunction with the other miRNA-AGO keeps the dissociated miRNA-AGO in close proximity to the site and thereby at a high local concentration, facilitating rebinding (Fig. 7, vertical axis). Likewise, the multivalent association of TNRC6 with the higher-order complex presumably helps prevent complete dissociation of TNRC6 (Fig. 7, horizontal axis). Thus, the entire TNRC6–$(\text{miRNA-AGO})_2$ complex has a slower dissociation from the target. With this slower dissociation, the repressive machinery associated with TNRC6 is tethered to the target mRNA for a longer period and thus has more time to deadenylate and translationally repress the target mRNA.

Although our experiments focused on targets bound to only one or two miRNA-AGO complexes, the ability of TNRC6 to simultaneously bind three complexes allows ready extension of the model to targets with three sites (8). Moreover, increased phase separation observed on the addition of AGO to a solution containing the TNRC6B AGO-binding domain suggests that AGO might have the ability to simultaneously interact with multiple TNRC6 molecules, albeit with presumably lower affinity to each molecule, which allows the model to extend to much higher-order complexes (6). Nonetheless, our results show that strong cooperative binding can be achieved without the formation of higher-order assemblies.

Materials and Methods

miRNA Duplexes. RNAs representing the guide and passenger strands of each miRNA duplex (*SI Appendix*, Table S1) were chemically synthesized (IDT). Passenger strands were synthesized with a 5′-monophosphate, whereas guide strands were synthesized with a 5′-OH. Guide strands were 5′-monophosphorylated using T4 polynucleotide kinase (New England BioLabs; M0201S) and a small amount of ATP [γ-^{32}P] (PerkinElmer; NEG035C001MC). The reaction was desalted with a P-30 column (Bio-Rad; 7326251). Each RNA was then purified on denaturing 15% acrylamide gel and resuspended in water. Two strands of a duplex were mixed with each other (870 pmol of each RNA) in annealing buffer (74 μL reaction with 30 mM Tris pH 7.5, 100 mM NaCl, and 1 mM EDTA) and then heated to 90 °C on a heat block, followed by cooling to 35 °C by sitting at room temperature for 90 min. NaCl was then added to a concentration of 0.39 M, and RNA was EtOH-precipitated and resuspended in 10 μL of annealing buffer. The duplex was then purified on a native 15% acrylamide gel that had been prerun for 10 min. Purified duplex RNA was EtOH-precipitated and resuspended in 10 μL of annealing buffer.

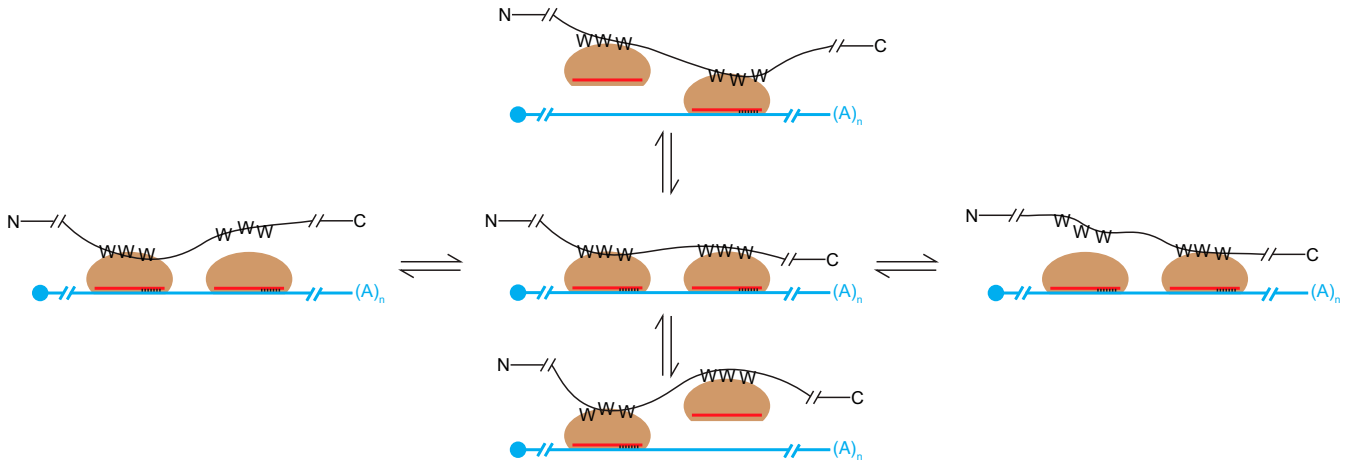

Fig. 7. Model for cooperative binding of both a two-site target (vertical axis) and TNRC6 (horizontal axis). Two AGO proteins (brown) loaded with miRNAs (red) associate with target mRNA (blue) that has cooperatively spaced target sites. TNRC6 (black) associates with both AGO proteins via TNRC6 tryptophan residues (W).

miRNA-AGO Preparation. Complexes of a specific miRNA-AGO were prepared as described previously, using an approach based on that of Flores-Jasso et al. (12, 14). The coding sequence of 3xFLAG-hAGO2 or 3xFLAG-hAGO1 was inserted into a pcDNA3.3 expression plasmid, and this plasmid was transfected into ∼90% confluent HEK293T cells using Lipofectamine 2000 in accordance with the manufacturer's instructions (pcDNA3.3–3XFLAG-AGO2, Addgene plasmid 136687; pcDNA3.3–3XFLAG-AGO1, Addgene plasmid 153556). After 2 d of growth, S100 cytosolic extract was harvested as described previously (13), except that cells were lysed in their hypotonic solution by being passed through a 23-gauge needle ∼20 times. S100 extract was then brought to 13% glycerol (wt/vol), snap-frozen in liquid nitrogen and stored in liquid nitrogen.

Gel-purified miRNA duplex was added to 1200 μL of S100 lysate to a final concentration of 50 nM. After incubating at 25 °C for 2 h to allow cellular machinery to load 3xFLAG-AGO, the lysate was added to 200 μL of a slurry of magnetic beads (Dynabeads MyOne Streptavidin C1; Invitrogen, 65001) prebound to 500 pmol of a 3′ biotinylated capture oligo bearing an 8-nt site to the miRNA (*SI Appendix*, Table S1), according to the manufacturer's protocol, except the washed oligo-bound beads were resuspended in equilibration buffer (18 mM Hepes pH 7.4, 100 mM KAc, 3 mM $MgAc_2$, 0.01% IGEPAL CA-630 [Sigma-Aldrich, I8896], 0.2 mg/mL BSA [New England BioLabs, B9000S], and 0.01 mg/mL yeast tRNA [Life Technologies, 15401-011]). After incubation at 22 °C for 1 h with agitation, beads were collected and washed five times in 400 μL of equilibration buffer and five times in 200 μL of high-salt equilibration buffer (18 mM Hepes pH 7.4, 2 M KAc, 3 mM $MgAc_2$, 0.01% IGEPAL CA-630, 0.2 mg/mL BSA, and 0.01 mg/mL yeast tRNA).

Captured miRNA-AGO complex was eluted by resuspending the beads in 200 μL of high-salt equilibration buffer containing 10 μM competitor DNA oligo (*SI Appendix*, Table S1), which was complementary to the capture oligo. After incubation at 22 °C for 2 h with agitation, the eluate was collected, supplemented with 50 μL of glycerol buffer (18 mM Hepes pH 7.4, 100 mM KAc, 1 mM $MgAc_2$, 0.01% IGEPAL CA-630, 0.2 mg/mL BSA, 0.01 mg/mL yeast tRNA, and 30% glycerol vol/vol), snap-frozen in liquid nitrogen, and stored at –80 °C.

Eluate was thawed and added to 20 μL of anti-FLAG M2 magnetic beads (Sigma-Aldrich; M8823), which had been prepared by washing three times with equilibration buffer. After incubation at 22 °C for 2 h with agitation, the beads were washed three times with 200 μL of equilibration buffer, then incubated in 60 μL of equilibration buffer supplemented with 146 μg/mL 3xFLAG peptide (Sigma-Aldrich; F4799) at 22 °C for 1 h with agitation. The eluate was collected, supplemented with 0.4 μL of 1 M DTT and 20.1 μL of 80% glycerol (vol/vol), snap-frozen in liquid nitrogen, and stored at –80 °C. Sequencing of small RNAs extracted from miRNA-AGO complexes prepared using this approach indicates that the desired miRNA comprises 97.7% to 99.5% of the miRNA loaded into each complex (12). miRNA-AGO2 concentrations were measured by filter binding, monitoring the fraction of labeled target bound in conditions in which the target was in excess over miRNA-AGO2 and in which both target and miRNA-AGO2 were far above the K_D of the interaction.

Cloning of 6B-ABD. pFRT/TO/FLAG/HA-DEST TNRC6B (Addgene plasmid 19884) (19) was a gift from Thomas Tuschl. TNRC6B residues 162 to 996 were amplified and appended to a His_6 tag using appropriate primers (*SI Appendix*, Table S1) (Q5 High-Fidelity DNA Polymerase; New England BioLabs; E0555S) and then inserted into the pMAL-c5X vector (New England BioLabs; N8108S) using Gibson assembly per manufacturer instructions (New England BioLabs; E5510S). Plasmids were transformed into NEB 5-alpha Competent *E. coli* cells (New England BioLabs; C2987I) and screened for the correct insert by Sanger sequencing. Verified plasmid was transformed into BL21DE3 *Escherichia coli* (Agilent; 200131) (pMAL-c5X-TNRC6B-ABD-His6; Addgene plasmid 153555). The next day, a colony was picked and used to generate a glycerol stock, which was stored at –80 °C.

Expression and Purification of 6B-ABD. A small scraping of glycerol stock was used to inoculate 5 mL of LB, which was grown under ampicillin selection at 37 °C overnight on a shaker. This 5-mL culture was then used to inoculate four 500-mL cultures of LB, which were grown under ampicillin selection at 37 °C on a shaker to an OD_{600} of 0.6. Cultures were transferred to 20 °C and induced with isopropyl β-D-1-thiogalactopyranoside (0.4 mM final concentration) and grown at 20 °C on a shaker overnight (∼16 h). Cultures were combined into two 1,000-mL bottles and centrifuged at 4,000 × *g* for 15 min at 4 °C. Pellets were resuspended in 50 mL of water and then centrifuged at 4,000 × *g* for 5 min at 4 °C. Pellets were resuspended in 47.5 mL of lysis buffer (20 mM Tris pH 7.5, 150 mM NaCl, 5% glycerol, 2 mM 2-mercaptoethanol, 0.1% IGEPAL CA-630, and cOmplete EDTA-free Protease Inhibitor Mixture [1 tablet per 50 mL of buffer; Roche; 11873580001]), and the suspension was sonicated six times (Branson Sonifier 250, 6 cycles of 50% output, 1 s on, 1 s off for 2 min) in a cold room on ice. Lysed samples were cleared by centrifugation at 50,000 × *g* for 30 min at 4 °C, and cleared lysate was added to Ni-NTA agarose beads (Qiagen; 30210), prepared by removing 500 μL of bead slurry, adding 2 mL of lysis buffer, centrifuging at 2,000 × *g* for 1 min, and removing supernatant. After gently rocking in a cold room at 5.5 °C for 105 min, samples were poured into a gravity-flow poly-prep chromatography column, which was washed with 25 mL of wash buffer (20 mM Tris pH 7.5, 150 mM NaCl, 5% glycerol, 20 mM imidazole pH 7.5, 2 mM 2-mercaptoethanol, and 0.1% IGEPAL CA-630).

Protein was eluted with 5 mL of elution buffer (20 mM Tris pH 7.5, 150 mM NaCl, 5% glycerol, 200 mM imidazole pH 7.5, 2 mM 2-mercaptoethanol, and 0.1% IGEPAL CA-630), and 4.7 mL of eluate was recovered and concentrated in a 100-kDa centrifugal filter unit (Amicon UFC910024) to 340 μl by centrifuging at 5000 *g* for 21 min at 4 °C. Then 160 μL of gel filtration buffer (18 mM Hepes pH 7.4, 100 mM KAc, 1 mM $MgAc_2$, 0.01% IGEPAL CA-630, 19.5% glycerol [vol/vol], and 5 mM DTT) was added to the concentrated sample, for a final volume of 500 μL. The concentrated sample was cleared by centrifugation at 21,130 × *g* for 5 min in a cold room at 5.5 °C and then transferred to a new tube.

The cleared sample was loaded onto a Superose 6 Increase 10/300 GL FPLC column (GE Life Sciences; 29091596) that had been preequilibrated with gel filtration buffer, and the column was run with gel filtration buffer on an ÄKTA pure fast protein liquid chromatograph, collecting 500-μL fractions.

Elution fractions taken at 14 to 15.5 mL, which included an A280 peak at 14.53 mL, were pooled. Fast protein liquid chromatography trace peak integration was used to estimate the eluate concentration from the extinction coefficient and molecular weight calculated at http://protcalc.sourceforge.net. Protein was aliquoted, snap-frozen in liquid nitrogen, and stored at –80 °C.

Mini-T6B and Mini-T6B_A Peptides. Peptides synthesized at purity ≥95% (GenScript) were resuspended in gel-filtration buffer, snap-frozen in liquid nitrogen, and stored at –80 °C.

Target RNAs. The two-site target RNA used exclusively in Fig. 1 was generated by in vitro transcription. In a 50-μL reaction, 1 μM top-strand DNA oligodeoxyribonucleotide and 1 μM bottom-strand template oligodeoxyribonucleotide (*SI Appendix*, Table S1) were incubated with 5 mM DTT, 8 mM GTP, 3.75 mM ATP, 3.75 mM CTP, 6.5 mM UTP, 40 mM Tris pH 7.9, 2.5 mM spermidine, 26 mM $MgCl_2$, 0.01% Triton X-100, and 5 μL of T7 polymerase (New England BioLabs; M0251L) at 37 °C for 2.5 h. Full-length RNA was purified on a denaturing gel and resuspended in water. Then 1 pmol of RNA was prepared for 5′ radiolabeling by dephosphorylation in a 20-μL reaction with rSAP (New England BioLabs; M0371S) according to the manufacturer's instructions. After incubation at 37 °C for 30 min, the enzyme was heat-inactivated at 70 °C for 5 min, and 1 μL of 115 mM DTT, 1 μL of ATP [γ-^{32}P], and 1 μL of T4 PNK were added. After incubation at 37 °C for 30 min, the reaction was desalted with a P-30 column, and labeled RNA was purified on a denaturing gel, with 15 μg of GlycoBlue (Invitrogen; AM9516) added as a coprecipitant during EtOH precipitation.

All other target RNAs were chemically synthesized (IDT) (*SI Appendix*, Table S1) and purified on denaturing gels. For each target, 1 pmol of purified 5′-OH RNA was radiolabeled with ATP [γ-^{32}P] and T4 PNK enzyme. After incubation at 37 °C for 1 h, the reaction was desalted with a P-30 column, and labeled RNA was purified on a denaturing gel, with 20 μg of linear acrylamide (Invitrogen; AM9520) added as a coprecipitant during EtOH precipitation.

Binding Reactions. Unless specified otherwise, binding reactions were performed with 5 pM target RNA in 18 mM Hepes pH 7.4, 100 mM KAc, 1.6 mM $MgAc_2$, 0.01 mg/mL yeast tRNA, 0.0029% IGEPAL CA-630, 0.058 mg/mL BSA, and 5 mM DTT. The binding reactions shown in Figs. 2 *B*, *C*, and *F*, 3*B*, 4 *B* and *E*, and 5*A* were performed in 20 mM Hepes pH 7.4, 110 mM KAc, 1.7 mM $MgAc_2$, 0.01 mg/mL yeast tRNA, 0.0039% IGEPAL CA-630, 0.058 mg/mL BSA, and 5 mM DTT. The binding reactions shown in Fig. 5*B* were performed in 22 mM Hepes pH 7.4, 120 mM KAc, 1.8 mM $MgAc_2$, 0.01 mg/mL yeast tRNA, 0.0049% IGEPAL CA-630, 0.058 mg/mL BSA, and 5 mM DTT. The binding reactions of Fig. 3*C* were performed in 18 mM Hepes pH 7.4, 100 mM KAc, 1 mM $MgAc_2$, 0.0043 mg/mL yeast tRNA, 0.01% IGEPAL CA-630, 0.043 mg/mL BSA, 5 mM DTT, and 18% glycerol. For reactions including 6B-ABD and/or mini-T6B, 6B-ABD, and mini-T6B were the last components added to the reaction mixture, with mini-T6B added after 6B-ABD in reactions including both. The reactions were incubated at 37 °C for 2 h.

Filter Binding. For each binding reaction, nitrocellulose (Amersham; Protran 10600062) and nylon (Amersham; Hybond-XL, catalog no. RPN 2020 S) filter paper disks (0.5-inch diameter) were equilibrated for 1 h in filter paper equilibration buffer (18 mM Hepes pH 7.4, 100 mM KAc, and 1 mM $MgAc_2$). The nitrocellulose disk was then stacked atop the nylon disk, which was placed atop a similar-sized circular pedestal. After application of 100 μL of filter paper equilibration buffer to the filter papers, the pedestal, with filter papers, was placed on a vacuum manifold (Visiprep SPE Vacuum Manifold; Supelco; 57250-U) set at approximately –7.5 inHg. After applying 10 μL of filter paper equilibration buffer as a blank to ensure proper vacuum suction, 10 μL of the sample was applied to the stacked filter papers. Filter papers were washed with 100 μL of ice-cold filter binding wash buffer (18 mM Hepes pH 7.4, 100 mM KAc, 1 mM $MgAc_2$, and 5 mM DTT), the pedestal with filter papers was removed from the apparatus, and the filter papers were separated, air-dried, and imaged on a phosphorimager (Typhoon FLA 7000 or Typhoon FLA 9500, GE Healthcare). Images were quantified using Multi Gauge software (Fuji Film) to assess the fraction of target bound by miRNA-AGO2.

To measure the concentration of purified miRNA-AGO2, a titration series of purified miRNA-AGO2 was added to 600 pM target RNA harboring a single 7-nt binding site and a 5′ monophosphate, some of which was radiolabeled. These data were fit to a saturation curve, which was used to infer the concentration of the miRNA-AGO2 complex. To measure K_D values, 5 pM RNA was combined with miRNA-AGO2 ranging from 0 to 600 pM in 10-μL reactions.

EMSA. When analyzing the same binding reaction with both filter binding and EMSA, 22 μL of reaction was prepared. Of this, 10 μL was used for filter binding, and the remaining sample was place on ice. After filter binding of all samples, the portions of binding reaction that remained were loaded (without loading dye) on a prechilled (2 h in a 5.5 °C cold room), prerun (10 min) native acrylamide gel (6% 29:1 acrylamide:bis-acrylamide, 7.8% glycerol, 89 mM Tris base, 89 mM boric acid, 2 mM EDTA, 18 mM Hepes pH 7.4, and 3 mM $MgCl_2$; running buffer: 89 mM Tris base, 89 mM boric acid, 2 mM EDTA, 18 mM Hepes pH 7.4, and 3 mM $MgCl_2$).

When analyzing a binding reaction with only EMSA, 11 μL of reaction was prepared, incubated at 37 °C for 2 h, placed on ice for 5 min, and then loaded on the gel. After running at 12 W for 90 min in the cold room (120 min for Fig. 3*C*), gels were the disassembled, the bottoms of unused flanking wells were marked by adding radioactive samples, and the gels were exposed on a phosphorimager screen at –20 °C overnight before imaging and quantification.

Competitive-Slicing Assay. miR-124–AGO2 was incubated with the two targets, with or without 2.22 nM 6B-ABD, at 37 °C for 2 h in a reaction volume of 12.6 μL (278 pM miR-124–AGO2, 55.6 pM each of the two target RNAs, 16.6 mM Hepes pH 7.4, 92.5 mM KAc, 0.924 mM $MgAc_2$, 0.0070 mg/mL yeast tRNA, 0.00425% IGEPAL CA-630, 0.020 mg/mL BSA, 8.02 mM DTT, and 9.76% glycerol). miR-1–AGO2 was then added, which brought the reaction volume to 14 μL (5 pM miR-1–AGO2, 250 pM miR-124–AGO2, 0 or 2 nM 6B-ABD, 50 pM each target RNA, 16.3 mM Hepes pH 7.4, 90.5 mM KAc, 0.905 mM $MgAc_2$, 0.00705 mg/mL yeast tRNA, 0.00455% IGEPAL CA-630, 0.0255 mg/mL BSA, 7.70 mM DTT, and 10.7% glycerol), and reactions were incubated at 37 °C. At the indicated time points, 2 μL was removed, added to 3 μL of denaturing loading dye (8 M urea, 25 mM EDTA), and placed on ice. Targets and sliced targets were resolved on 15% denaturing gels and quantified using a phosphorimager.

Dissociation Assay. Two-site target RNA was incubated with miR-1–AGO2 with or without 2 nM 6B-ABD at 37 °C for 2 h in 40 μL (10 pM target RNA, 20 pM miR-1–AGO2, 18 mM Hepes pH 7.4, 100 mM KAc, 1 mM $MgAc_2$, 0.001 mg/mL yeast tRNA, 0.01% IGEPAL CA-630, 0.001 mg/mL BSA, 5 mM DTT, and 6% glycerol). Meanwhile, 665 μL of dilution buffer (18 mM Hepes pH 7.4, 100 mM KAc, 1 mM $MgAc_2$, 0.01% IGEPAL CA-630, 5 mM DTT, and 0.08% glycerol, with or without 2 nM 6B-ABD), was preincubated at 37 °C for 15 min, while 95 μL of the same buffer was placed on ice for 15 min. For the 0-min time point, 5 μL of the reaction was mixed with the 95 μL of ice-cold buffer, and the 100-μL reaction mix was immediately filtered through stacked membranes, followed by a wash with 200 μL of ice-cold filter binding wash buffer. For the other time points, the remaining 35 μL of reaction was diluted into the preincubated 665 μL of dilution buffer, and at each time point 100-μL aliquots were removed and filtered through stacked membranes, followed by a wash with 200 μL of ice-cold filter binding wash buffer. Data from filters that failed due to vacuum-seal issues were discarded (6 out of 42). After the 20-fold dilution, reaction components were as follows: 0.5 pM RNA, 1 pM miR-1–AGO2, 0.00005 mg/mL yeast tRNA, 0.0005 mg/mL BSA, and 0.38% glycerol, with all other components remaining at their starting concentrations.

Fitting Curves to Data. Equations for specific binding to one-site and for specific binding to multiple sites with Hill slope were fit to data using GraphPad Prism. For Fig. 6*D*, a linear equation was fit to the competitive-slicing data and graphed in R. For Fig. 6*G*, a single exponential equation with a nonzero final equilibrium was fit to the dissociation assay data and graphed in R.

Data Availability. All relevant data, protocols, and informatics analysis are available in the main text and *SI Appendix*.

ACKNOWLEDGMENTS. We thank S. E. McGeary, D. H. Lin, and others in the D.P.B. laboratory for helpful discussions, and T. M. Pham for purification of the miR-124–AGO1 complex. This work was supported by a grant from the NIH (GM118135). D.P.B. is an investigator of the Howard Hughes Medical Institute.

1. D. P. Bartel, MicroRNAs: Target recognition and regulatory functions. *Cell* **136**, 215–233 (2009).
2. A. O. Subtelny, S. W. Eichhorn, G. R. Chen, H. Sive, D. P. Bartel, Poly(A)-tail profiling reveals an embryonic switch in translational control. *Nature* **508**, 66–71 (2014).
3. S. Jonas, E. Izaurralde, Towards a molecular understanding of microRNA-mediated gene silencing. *Nat. Rev. Genet.* **16**, 421–433 (2015).
4. S. W. Eichhorn *et al*., mRNA destabilization is the dominant effect of mammalian microRNAs by the time substantial repression ensues. *Mol. Cell* **56**, 104–115 (2014).
5. T. J. Eisen, S. W. Eichhorn, A. O. Subtelny, D. P. Bartel, MicroRNAs cause accelerated decay of short-tailed target mRNAs. *Mol. Cell* **77**, 775–785.e8 (2020).
6. J. Sheu-Gruttadauria, I. J. MacRae, Phase transitions in the assembly and function of human miRISC. *Cell* **173**, 946–957.e16 (2018).
7. J. Pfaff *et al*., Structural features of Argonaute-GW182 protein interactions. *Proc. Natl. Acad. Sci. U.S.A.* **110**, E3770–E3779 (2013).
8. E. Elkayam *et al*., Multivalent recruitment of human Argonaute by GW182. *Mol. Cell* **67**, 646–658.e3 (2017).
9. R. C. Friedman, K. K. Farh, C. B. Burge, D. P. Bartel, Most mammalian mRNAs are conserved targets of microRNAs. *Genome Res.* **19**, 92–105 (2009).
10. A. Grimson *et al*., MicroRNA targeting specificity in mammals: Determinants beyond seed pairing. *Mol. Cell* **27**, 91–105 (2007).
11. P. Saetrom *et al*., Distance constraints between microRNA target sites dictate efficacy and cooperativity. *Nucleic Acids Res.* **35**, 2333–2342 (2007).
12. S. E. McGeary *et al*., The biochemical basis of microRNA targeting efficacy. *Science* **366**, eaav1741 (2019).
13. L. M. Wee, C. F. Flores-Jasso, W. E. Salomon, P. D. Zamore, Argonaute divides its RNA guide into domains with distinct functions and RNA-binding properties. *Cell* **151**, 1055–1067 (2012).
14. C. F. Flores-Jasso, W. E. Salomon, P. D. Zamore, Rapid and specific purification of Argonaute-small RNA complexes from crude cell lysates. *RNA* **19**, 271–279 (2013).
15. W. E. Salomon, S. M. Jolly, M. J. Moore, P. D. Zamore, V. Serebrov, Single-molecule imaging reveals that Argonaute reshapes the binding properties of its nucleic acid guides. *Cell* **162**, 84–95 (2015).
16. K. Takimoto, M. Wakiyama, S. Yokoyama, Mammalian GW182 contains multiple Argonaute-binding sites and functions in microRNA-mediated translational repression. *RNA* **15**, 1078–1089 (2009).
17. J. Hauptmann *et al*., Biochemical isolation of Argonaute protein complexes by Ago-APP. *Proc. Natl. Acad. Sci. U.S.A.* **112**, 11841–11845 (2015).
18. G. R. Chen, H. Sive, D. P. Bartel, A seed mismatch enhances argonaute2-catalyzed cleavage and partially rescues severely impaired cleavage found in fish. *Mol. Cell* **68**, 1095–1107.e5 (2017).
19. M. Landthaler *et al*., Molecular characterization of human Argonaute-containing ribonucleoprotein complexes and their bound target mRNAs. *RNA* **14**, 2580–2596 (2008).